Available online at www.sciencedirect.com
ScienceDirect
Icarus 192 (2007) 77–91
ICARUS
www.elsevier.com/locate/icarus

Mountains on Titan observed by Cassini Radar

Jani Radebaugh [a,d,*], Ralph D. Lorenz [b,d], Randolph L. Kirk [c], Jonathan I. Lunine [d,e], Ellen R. Stofan [f], Rosaly M.C. Lopes [g], Stephen D. Wall [g], the Cassini Radar Team

[a] *Department of Geological Sciences, Brigham Young University, Provo, UT 84602, USA*
[b] *Space Department, Planetary Exploration Group, Johns Hopkins University Applied Physics Laboratory, Laurel, MD 20723, USA*
[c] *United States Geological Survey Astrogeology Division, Flagstaff, AZ 86001, USA*
[d] *Lunar and Planetary Laboratory, University of Arizona, Tucson, AZ 85721, USA*
[e] *INAF-IFSI, Via del Fosso del Cavaliere, 100, Rome 00133, Italy*
[f] *Proxemy Research, 14300 Gallant Fox Lane, Suite 225, Bowie, MD 20715, USA*
[g] *Jet Propulsion Laboratory, California Institute of Technology, 4800 Oak Grove Drive, Pasadena, CA 91109-8099, USA*

Received 30 June 2006; revised 8 June 2007
Available online 11 August 2007

Abstract

The Cassini Titan Radar mapper has observed elevated blocks and ridge-forming block chains on Saturn's moon Titan demonstrating high topography we term "mountains." Summit flanks measured from the T3 (February 2005) and T8 (October 2005) flybys have a mean maximum slope of 37° and total elevations up to 1930 m as derived from a shape-from-shading model corrected for the probable effects of image resolution. Mountain peak morphologies and surrounding, diffuse blankets give evidence that erosion has acted upon these features, perhaps in the form of fluvial runoff. Possible formation mechanisms for these mountains include crustal compressional tectonism and upthrusting of blocks, extensional tectonism and formation of horst-and-graben, deposition as blocks of impact ejecta, or dissection and erosion of a preexisting layer of material. All above processes may be at work, given the diversity of geology evident across Titan's surface. Comparisons of mountain and blanket volumes and erosion rate estimates for Titan provide a typical mountain age as young as 20–100 million years.

Keywords: Titan; Satellites, surfaces; Saturn, satellites; Tectonics

1. Introduction

The Cassini spacecraft, with its ensemble of instruments designed to peer through the hydrocarbon haze enshrouding Saturn's largest moon, Titan, has revealed a diverse array of geological features on Titan's surface. The Cassini Titan Radar Mapper (hereafter, Cassini Radar) has observed dunes (Lorenz et al., 2006a, 2006b; Elachi et al., 2006a; Radebaugh et al., 2007), lakes (Stofan et al., 2007), cryovolcanic features (Elachi et al., 2005, 2006a; Lopes et al., 2007), river-like channels (Lorenz et al., 2007a; Lunine et al., 2007), and degraded impact craters (Elachi et al., 2006a; Stofan et al., 2006; Wood et al., 2005; Lorenz et al., 2007b). The Cassini Radar has also discovered features of relatively high topography that we refer to as mountains (Radebaugh et al., 2006), and whose topography we analyze here.

The dominant topographic forms on the only two moons of comparable size and mass to Titan, Ganymede and Callisto, are impact craters and Ganymede's grooved terrain. Hence, just prior to Cassini it was assumed that most of the topography would be dominated by impact structures, so that mountains and mountain ranges would be central peaks and rims of craters, with low-lying impact crater basins perhaps filled with liquid methane that had periodically rained out of the atmosphere (Lorenz and Lunine, 2005; Lorenz and Mitton, 2002; etc). Cassini has revealed that impact structures are sparse

* Corresponding author. Fax: +1 801 422 0267.
E-mail address: jani.radebaugh@byu.edu (J. Radebaugh).

0019-1035/$ – see front matter
doi:10.1016/j.icarus.2007.06.020

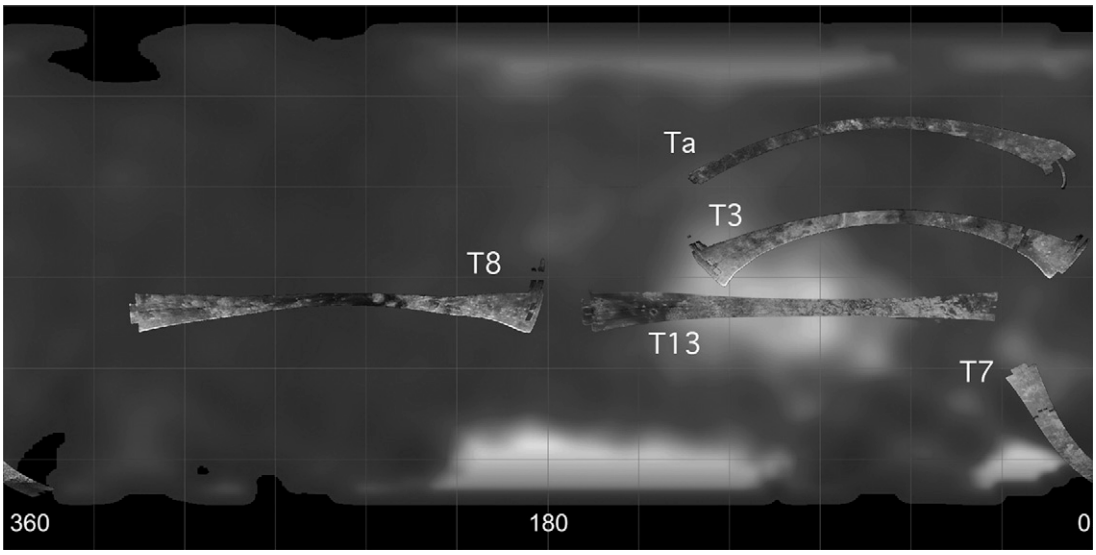

Fig. 1. Cassini Radar SAR coverage of Titan over the mountainous areas discussed in this paper, as well as previous and intervening swaths (coverage through May 2006). Swaths referred to in this work, Ta, T3, T7, T8, and T13, are shown. These image swaths cover ∼8% of Titan's surface at widely varying locations at ∼1 km px^{-1} resolution.

(Porco et al., 2005; Elachi et al., 2005, 2006a; Stofan et al., 2006; Lorenz et al., 2007b). Instead, it appears that Earth-like processes, perhaps with a complex "methanological" cycle that includes rainout, fluvial erosion (Tomasko et al., 2005; Lorenz et al., 2007a) and reevaporation, have shaped Titan's surface into a much more Earth-like landscape than was expected. Overall, Titan's topography is subdued, with amplitudes of a few hundred meters in the small fraction of the surface covered by altimetry (Elachi et al., 2005, 2006a; Callahan et al., 2006), and stereo image pairs from Huygens (Tomasko et al., 2005). Interestingly, topography of this amplitude was predicted for Titan's surface based on atmospheric gravity wave analysis (Friedson, 1994). We desire to know what forces shaped Titan's presumed-icy crust and led to the surface topography we see. In addition to the geological and geophysical interest, we also note that future exploration of Titan may involve aerial platforms such as balloons (Tokano and Lorenz, 2006) and thus the characterization of mountain area, distribution and height is important in defining the topographic hazards to such vehicles.

We use data from Cassini Radar operating at 2.17 cm wavelength in synthetic aperture radar (SAR) mode (Elachi et al., 2005) to study features that reveal topography in the form of closely paired bright and dark image areas, indicative of radar illumination across a sharp topographical boundary. Images have range and azimuth resolutions of 300 to 1500 m, although the image products we analyze are oversampled to obtain 175 m pixel^{-1} (256 pixels per degree) ground sample distance. Current radar swath coverage of Titan is shown in Fig. 1.

Available techniques for estimating topographic relief include altimetry, stereogrammetry, and shape-from-shading. As discussed, radar altimeter data cover only a limited area of Titan, to date in areas for which high-resolution imaging is not available, hindering interpretation of the results. The resolution of optical images is inadequate to assess the low relief found so far on Titan by stereo methods, but the Cassini Radar will return overlapping images of a few areas of Titan with excellent stereo geometry. At the time this is written, however, such observations are just beginning. Fortunately, the radar images already obtained are well suited to detecting topographic relief from its shading effects and making quantitative estimates by shape-from-shading (or radarclinometry). The Radar is far better suited than optical remote sensing instruments on the Orbiter for this purpose, because absorption and scattering of light in Titan's thick, hazy atmosphere leads to diffuse surface illumination which makes contrasts in the optical images too weak for photoclinometry. Indeed, no appreciable shadows are cast, and evidence for topographic shading in the optical images is ambiguous. (By operating below the bulk of the atmospheric haze, the DISR instrument on the Huygens probe was able to provide high resolution topography via stereo pairs created as it drifted past features, but over a very limited patch of terrain only; Tomasko et al., 2005.) Thus, we rely on the imposed shading created by the radar illumination process to reveal topography, and quantify relief with models, based on theory and instrument design, that take account of the relationship between radar brightness and slope.

In this paper, we use data obtained during Cassini's T3 flyby in February 2005, the T8 flyby in October 2005, and isolated data from the T13 flyby in April 2006 to find the heights, morphologies, and locations of mountains within these regions on Titan. Few discrete mountain features were seen in the TA data (October 2004) and in the T7 swath (September 2005). Extensive ranges of mountains were seen in the T13 swath (May 2006) within the Xanadu region, where we have measured just a few features thus far, and some isolated mountains are seen in other regions on Titan in later swaths. Since new radar swaths are continually being obtained, and new sets of mountains are being observed, this paper should be considered a discovery paper, containing data for those select regions mentioned above

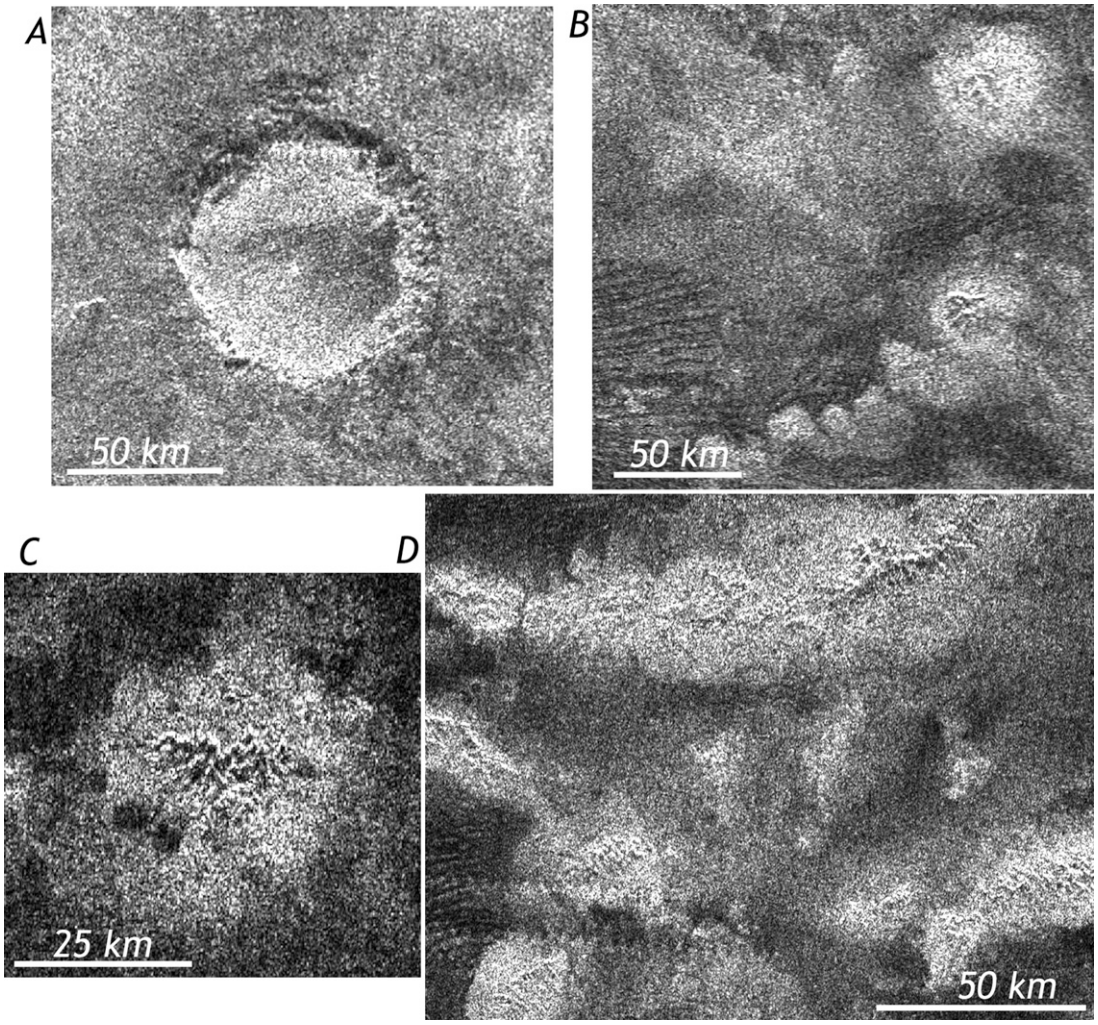

Fig. 2. Some examples of mountains on Titan. Radar illumination is from the top in all cases, and north is up. Bright, possibly erosional, blankets surround the central, high elevation features visible as bright/dark pairs. (A) Sinlap Crater, shown to demonstrate the effects of radar illumination on a rimmed depression. (B) Individual mountain blocks in the T3 Area A (see Fig. 4) south of Sinlap crater. (C) Rugged mountain from the middle of T3 Area B (see Fig. 4). (D) A portion of mountain ranges west of the Huygens landing site seen in the T8 swath.

along with preliminary discussions of possible formation mechanisms.

2. Features and study areas

The features under study in the Radar swaths T3, T8, and T13 are small regions (usually under 20 km across) that are elevated above the surrounding terrain. In passing, we note the application of the term 'mountains' to certain, low-amplitude features found on the Earth's US desert southwest (see Section 4.2) and follow that usage here. Although the Titan topography may be modest compared with the largest mountains on Io, Mars, or Earth, when compared to the very subdued topography we observe elsewhere on Titan (e.g., Elachi et al., 2005) the features in this paper are indeed 'mountains.'

Mountains observed in the Radar swaths exhibit high topography as inferred from radar shading. Evidence that these features are indeed topographic, that is, that their appearance is affected primarily by the illumination angle of the surface rather than by spatial variation of compositional or scattering properties, comes from the close pairing of light and dark regions in the crosstrack direction. Our interpretation of the bright and dark areas as radar-facing and away-facing slopes is supported by the fact that the bright areas are generally narrower, consistent with the geometric distortion inherent in radar imaging (foreshortening and layover) (e.g., Stofan et al., 1993). Several examples of mountains we have studied are shown in Fig. 2, with an impact crater for comparison, to help illustrate the bright/dark pairing associated with topography.

Strong bright/dark signals are apparent in the centers of features in Figs. 2B and 2C. These isolated features have a long, meandering morphology, often with double or triple subparallel crests that occasionally intersect (Fig. 2C). Some features join up in much longer, chain-like "ranges" that can extend several hundred kilometers. These features also often demonstrate multiple crests instead of a single peak (Fig. 2D). The mountains on Titan do not resemble wrinkle ridges on Venus, the Moon, and other planetary bodies (e.g., Solomon et al., 1992), nor do they appear to be simple ridge/fold structures or horsts and grabens. Rather, they somewhat resemble folded

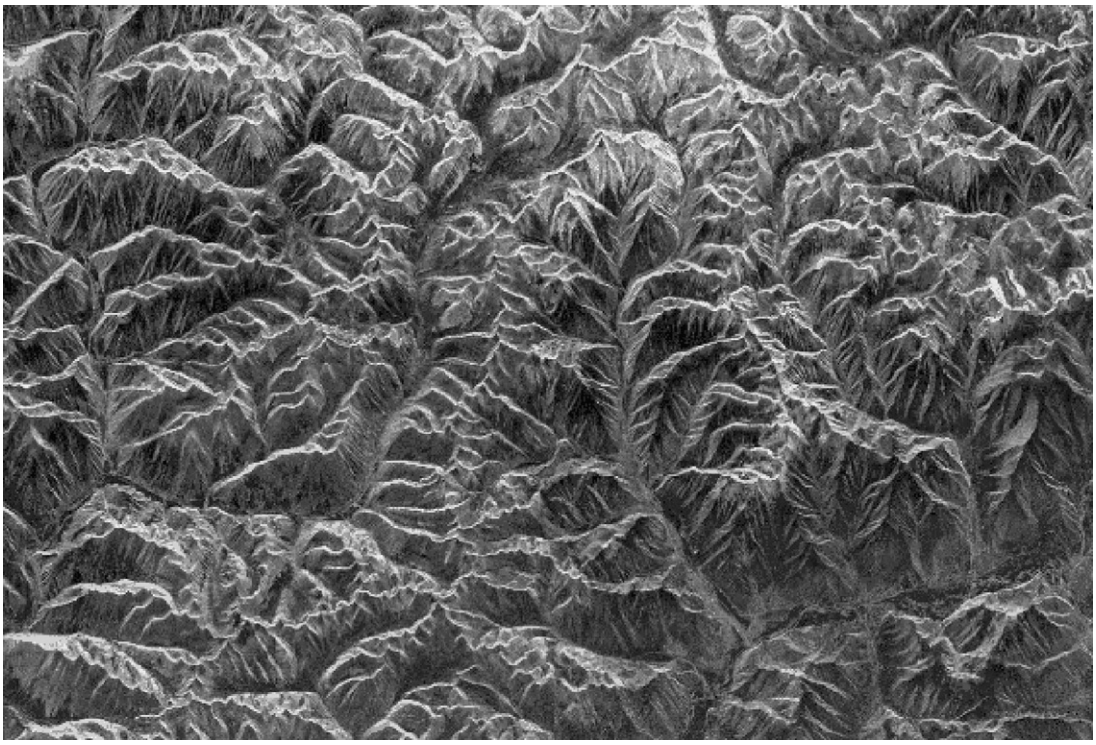

Fig. 3. Radar image of the Tibetan Himalayas acquired by the Spaceborne Imaging Radar-C/X-band Synthetic Aperture Radar (SIR-C/X-SAR) on April 10, 1994, on board the space shuttle Endeavour. North is toward the upper left, image is 49.8 km by 33.6 km and is centered at 30.2° N latitude, 92.3° E longitude. Elevation varies by 1500 m in the scene, in comparison with close to 1000 m for the Titan images. Note the meandering, sub-parallel ridges bear a resemblance to the ridge top in Fig. 2C, although the terrestrial image is close to 10 m/pixel resolution, compared with 175 m/pixel for the Titan images. More information can be found at http://www.jpl.nasa.gov/radar/sircxsar/tibet.html. Image courtesy of NASA/JPL-Caltech.

mountain belts on Earth that have been subject to erosion. For example, the Tibetan Himalayas imaged by spaceborne radar have a few points in similarity to mountains on Titan, in that there are meandering, sub-parallel, crested ridges. The terrestrial examples shown here are the result of rapid uplift and extensive erosion by water and glacial action (e.g., Gupta et al., 2006) (Fig. 3).

The T3 flyby, which occurred in February 2005, produced a SAR swath that covered a region just north of the equator, from 3° S–23° N latitude and 0°–133° W longitude, about 2% of Titan's surface (Elachi et al., 2006a). Mountains are found in two main regions in the T3 swath, with unique morphologies exhibited in each region. Mountains in eastern T3, or Area A (Figs. 4 and 5), are generally isolated blocks found in apparently flat plains. Radar-brighter, diffuse materials surround the mountain margins. These are presumably materials of slightly different grain size or composition than the surrounding, dark plains. These might be blankets of materials eroded from the mountains, slightly elevated above the plains, perhaps analogous to bajadas in western US deserts. Copious dark dunes typically 1–2 km wide and tens of kilometers long run predominantly W–E and abut and divert around obstacles, such as the margins of the mountains. The dunes indicate that winds blow in this region with a cumulative W–E direction (Boubin et al., 2005; Lorenz et al., 2006a, 2006b; Elachi et al., 2006a; Radebaugh et al., 2007). The diffuse material surrounding many of the mountains also trails out to the east, indicating that this material was unconsolidated and was also blown by the winds in this region. These diffuse deposits are best explained as mountain material that has been eroded (by fluid flow and/or mass wasting) and was then entrained and redeposited by eolian processes.

Mountains in the center of the T3 swath, or Area B (Figs. 4 and 5), form long, linear chains with some surrounding, isolated blocks. Diffuse, blanket-like deposits also surround the mountains in this area. In Area B—planimetric streaks that may indicate the paths of erosion-modified flow direction are not as strong as in T3 Area A, nor are dunes as prominent in Area B (Elachi et al., 2006a).

The T8 flyby, which occurred in October 2005, produced a SAR swath of a region just below the equator, from ∼200°–320° W and 5°–20° S (Lunine et al., 2007). Mountains in the T8 swath (Fig. 5C) are curvilinear in planform, have an overall E–W orientation, and form ranges that extend several hundred kilometers. These also have diffuse blankets surrounding their peaks.

The T13 swath, obtained April 2006, includes parts of the optically and radar-bright province Xanadu, at ∼90°–150° W and 20° S–10° N. This province contains many mountains, often grouped together as summits atop broad, high plateaus, similar to the Himalayan plateau (Fig. 3).

3. Heights and slopes

As an initial survey of mountainous features seen in the radar swaths from T3 and T8, we measured heights and slopes of the

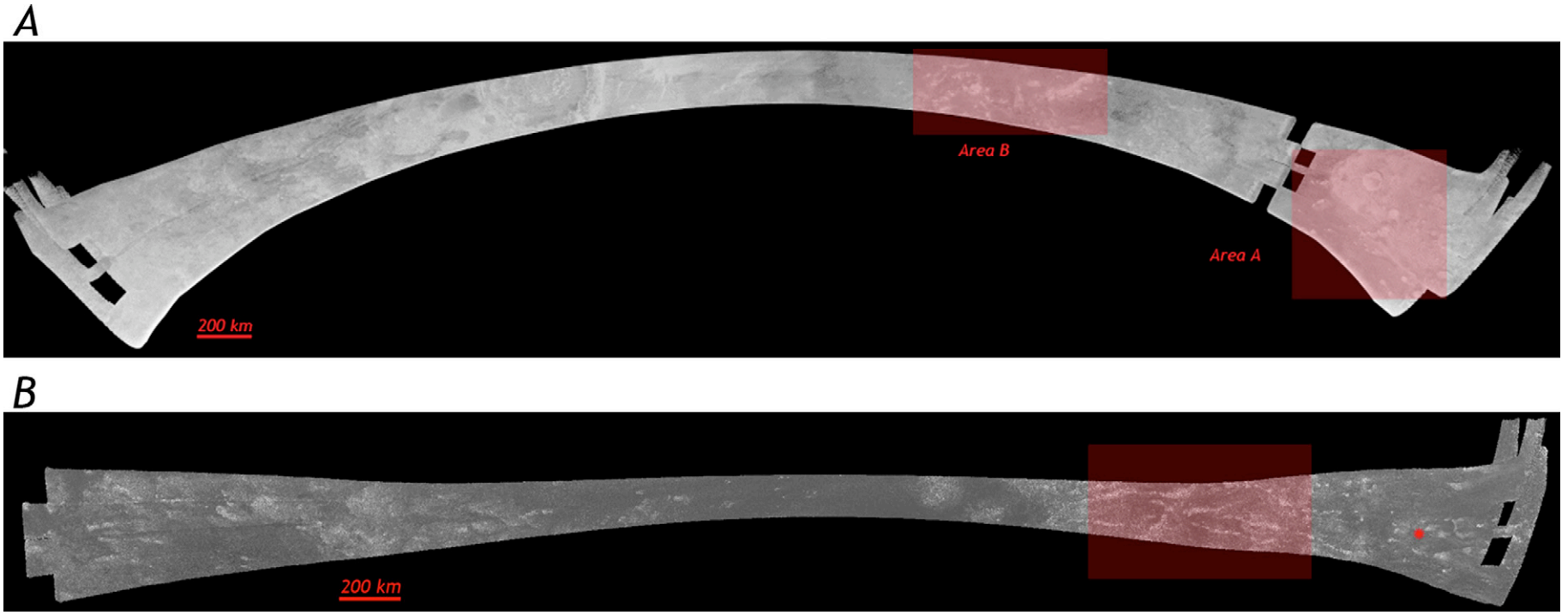

Fig. 4. (A) T3 swath with mountain study areas outlined. (B) T8 swath with mountain study area outlined. Red star on eastern end marks the Huygens landing site. See Fig. 5 for close-ups of highlighted regions. Other mountainous regions can be seen in both image swaths outside the study areas. However, many of these features either were associated with the impact crater in the central-west region of the T3 swath or had insufficient topography to obtain accurate height measurements.

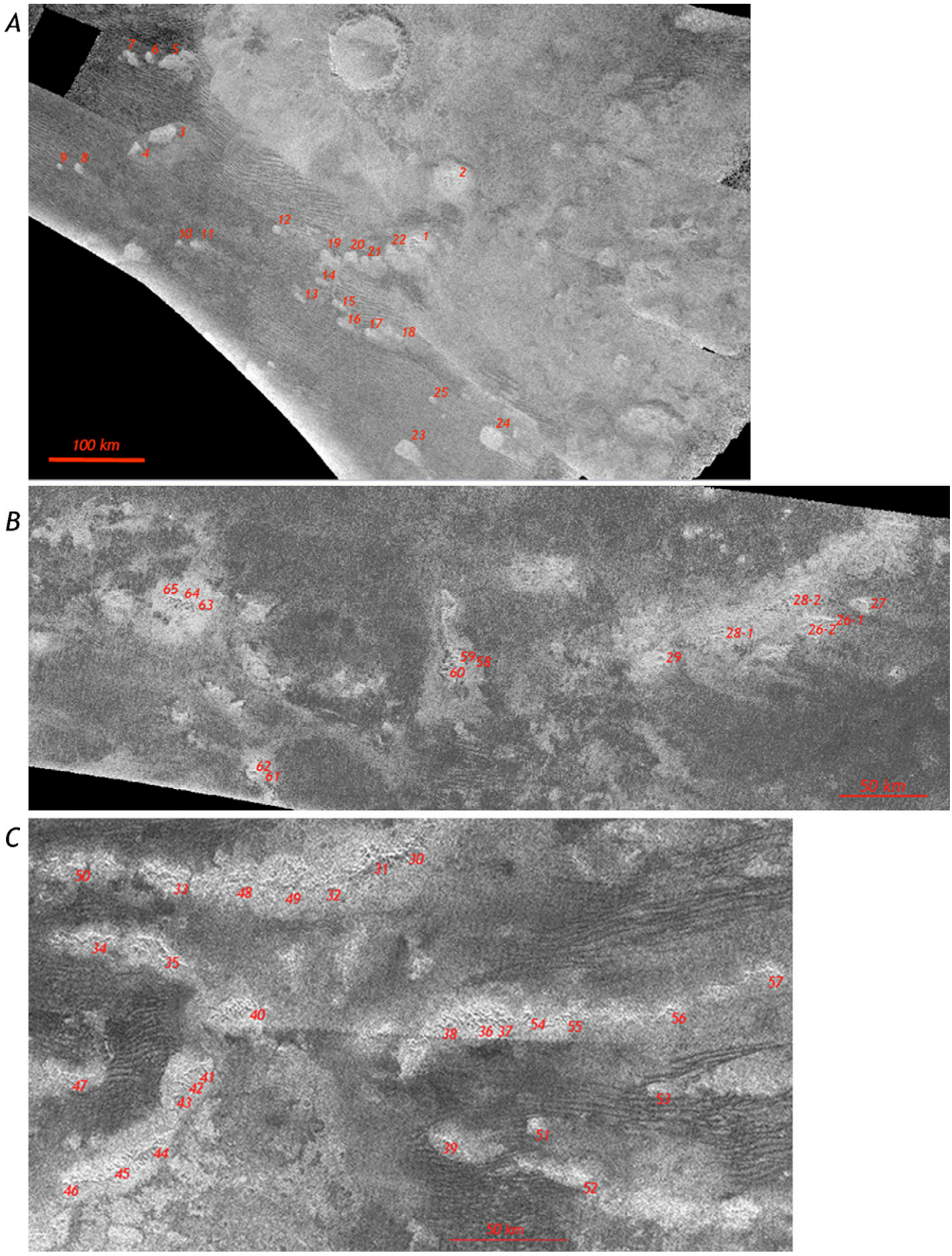

Fig. 5. (A) Mountain blocks measured near Sinlap impact crater in the T3 Area A (far east) of Fig. 4A. (B) Mountains measured in the T3 Area B (middle region) of Fig. 4. Because the mountains are more chain-like, multiple peaks along a single chain were measured. (C) Mountains measured in the T8 swath study area (center-right) of Fig. 4. Multiple peaks along a single range were also measured in this region. Scales are all different; north is up in all cases.

most prominent features of high topography in the study areas using the technique of radarclinometry, or shape-from-shading.

3.1. Radarclinometry method

Radarclinometry is based on the quantitative interpretation of brightness variations as slopes, based on an assumed model backscatter law, followed by the integration of slopes to obtain topography. Because most of the mountains studied here are rather small in extent, and because it is their peak height that is of greatest interest, we have primarily utilized a simple, one-dimensional radarclinometry technique to construct elevation profiles across the mountains (Kirk et al., 2005). In order to obtain a one-to-one correspondence between backscatter and the slope along the profile, we neglect the smaller influence of cross-profile slopes on the signal and simply set these slopes to zero. In the T13 image of Xanadu (where larger areas of mountains with uniform scattering properties are found), our profiling results agree with digital topographic models constructed by two-dimensional radarclinometry (Kirk, 1987; Kirk et al., 2006), which takes cross-slopes into proper account.

For radarclinometry to yield a quantitatively accurate estimate of topography, the backscatter model used must closely match the scattering behavior of the actual surface. In our early work (Kirk et al., 2005; Radebaugh et al., 2006), we used a law of the form $\sigma_0(i) \propto \cot(i)$, which closely fits the backscatter of uniform radar-dark plains as measured from the SAR images over a wide range of incidence angles i (Kirk et al., 2005). More recently, however, the T13 dataset has revealed that the mountainous areas of Xanadu, which are much brighter than the plains, have a nearly constant backscatter $\sigma_0(i)$ over a range of incidence angles $1° \leqslant i \leqslant 30°$ from the near to far edge of the image swath (Kirk et al., 2006). Cassini Radar observations of Xanadu obtained in scatterometry mode support this conclusion, and are well fit by a standard diffuse scattering law of the form $\sigma_0(i) \propto \cos(i)$ (Wye et al., 2007). These scatterometry observations do not yet extend to small incidence angles, so it is currently unknown whether the backscatter behavior of Xanadu is purely diffuse (roughly constant as i decreases) or contains a contribution from quasi-specular surface reflection (backscatter increasing as i decreases). The extremely depolarized thermal emission from Xanadu (Paganelli et al., 2007a, 2007b) argues against a significant quasi-specular reflection.

In our present work, we adopt a purely diffuse scattering law $\sigma_0(i) \propto \cos(i)$ for all mountains. Unlike Xanadu, the mountains observed earlier are so small that each is effectively sampled at a single incidence angle, but the ensemble of all observations indicates that these features are radar bright regardless of incidence angle. An estimate of σ_0 of each mountain at the incidence angle of a level surface is obtained as part of the modeling process; this parameter of the scattering law is determined by "leveling" the profile so the near and far bases of the mountain have the same elevation. (Note the implicit assumption that the scattering properties do not vary significantly over the profile due to compositional or textural differences. For short distances of km or a few tens of km within a single surface unit, such variations are indeed small compared to the slope-related backscatter variations, but over longer profiles and more heterogeneous terrains the variations in scattering behavior can become more important and the topographic results must be viewed with caution.) The resulting backscatter estimates are systematically bright both for Xanadu and for mountains elsewhere, with a mean of 1.0 in T8 and 1.5 in T3 and T13 compared to ∼0.25 for the dark plains at comparable incidence angles. Any systematic variation in cross-section with incidence angle is small compared to the random variation between different mountains. We thus conclude that the diffuse scattering law initially derived for Xanadu is appropriate for all mountains. The consequence of substituting this model for the more strongly varying cot law used previously is to increase the estimated heights of all features by roughly a factor of 2. We have also tested the effect of including a plains-like quasi-specular contribution in addition to the diffuse term. The result is to decrease the heights and slopes reported below by 10–15%.

3.2. Results

Most mountains in our study regions are fairly subtle features (Fig. 6). Peaks in all regions range from 120 m to just over 1000 m in uncorrected (see below) estimated height with means of 380, 570, and 420 m in T3 Area A, T3 Area B, and T8, respectively. The overall uncorrected mean is 440 m. Our topographic profiles range from 5 to 20 km in length, so typical slopes are also rather gentle. We have tabulated statistics on extreme slopes, but also (because these may be unduly influenced by speckle noise brightening or darkening individual pixels) on slopes averaged over relatively straight (i.e., nearly uniform) stretches on each side of the peak.

In the examples in Fig. 6, the mountain with low slopes is relatively symmetric but the steeper mountain is distinctly asymmetric. This observation holds generally, and is crucial to the interpretation of all our results. [We initially reported (Radebaugh et al., 2006) that slopes in T3 Area A were low and relatively symmetric, but this result was not representative of a larger sample of Titan's mountains.] Fig. 7 compares the averaged slopes on the bright (radar-facing) and dark (away-facing) slopes of all mountains studied. Bright slopes can be comparable to dark ones when both are less than about 10°, but, whereas dark slopes approach 65° in some cases, bright slopes increase only gradually and never exceed about 20°. The relation between slopes follows a single, consistent trend in all regions studied, so it is improbable that it results from a true asymmetry of Titan's mountains. If that were the case, we would expect to see at least some areas where the radar-facing slope is the steepest.

Instead, the pattern observed in Fig. 7A can be explained consistently in terms of the finite resolution of the radar images. Radar imaging locates features by their range to the spacecraft, but the images are created in map projection by assuming that all these features fall on a constant-elevation spherical surface. Thus, peaks seem to "lean" away from the radar. If the mountain is well resolved, then we can undo this distortion by calculating the true horizontal coordinate of its peak from the range and

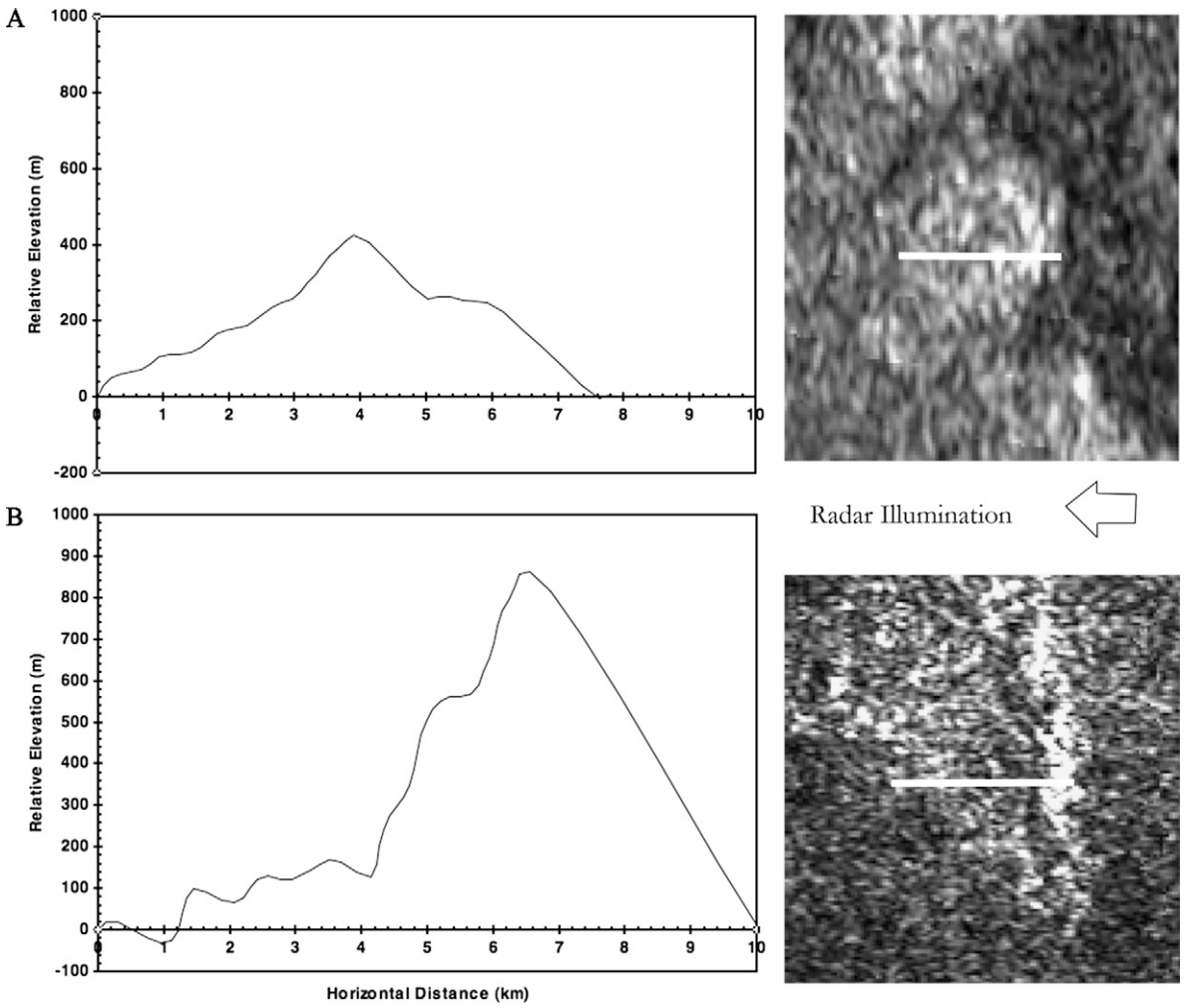

Fig. 6. Radarclinometric trace across two mountains in the T3 swath, one (top, A) Mountain 21 from Area A near Sinlap Crater and one (bottom, B) Mountain 26-1 from T3 Area B near the middle (see Fig. 5A for context). Line through the mountain image denotes the pixel trace where data was obtained. Graphs show mountain heights to the same scale in the form of a cross section through the mountain, with vertical exaggeration. The high mountain (B) shows marked "leaning" toward the left, due to understeepening of the bright side slope from resolution effects (see Section 3.2 for discussion).

height. If, however, the foreshortened bright side of the feature appears broadened because of the image resolution, this bright side will be too wide (and its slope will be underestimated) in the reconstructed profile. This qualitative argument is supported by detailed, albeit somewhat idealized, modeling (Kirk et al., 2006; Kirk and Radebaugh, 2007). It is straightforward to calculate how an idealized, symmetric hill (in cross-section, an isosceles triangle) would appear in a radar image of given resolution and incidence angle, and, from this, how it would be reconstructed by our radarclinometry algorithm. The modeling and reconstruction can be done even when the slopes exceed the incidence angle relative to the horizontal surface, so that the bright slope is not merely foreshortened but "folded over." For the diffuse cos scattering law, the results are extremely simple: the dark slope is always equal to the true slope, but the bright slope is increasingly underestimated as the slope increases, the incidence angle decreases, or the resolution becomes worse.

Thus, the distribution of inferred dark slopes (Fig. 7B) should reflect the true slope distribution. Averaged dark slopes range from 4.1° to 60.4° with a mean of 28.2°. Extreme dark slopes average 37.2° and are found as large as 63.9°, but, as noted, this may reflect the sensitivity of the radarclinometry method to noise rather than actual slopes.

Our idealized hill models, which we assert best describe the actual hills, also predict how much the height of a hill will be underestimated. Because the dark-side slope estimated by radarclinometry is nearly the true slope on both sides of the hill, it is straightforward to calculate the true height of a triangular hill from the dark slope and the width of the base. To estimate corrected heights of our real hills, which are not precisely triangular, we calculate a correction factor based on the average slopes of straight segments on the bright and dark sides, then apply this correction to the profile as a whole. The results are shown in Fig. 8, which is a scatterplot of corrected height on the abscissa and uncorrected height on the ordinate paired with a histogram of corrected heights. The mean corrected height is 864 m and mountains range in height from 123 to 1930 m. In this preferred analysis of slopes and elevations, the highest mountains nearly reach 2000 m.

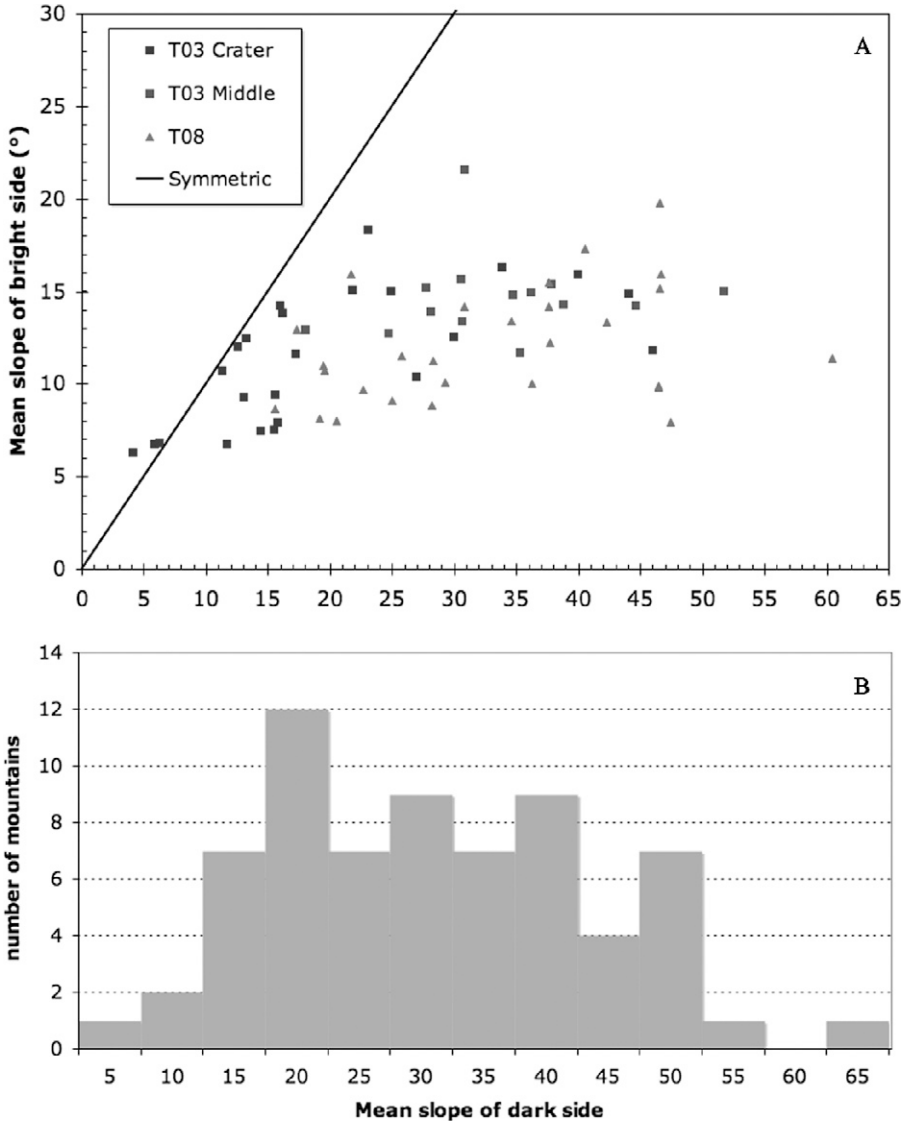

Fig. 7. (A) Mean bright (uprange) and dark (downrange) slopes are plotted for each mountain measured. The deviation from symmetry toward steeper downrange slopes indicates there is some layover, and calculated mountain heights are likely somewhat below actual heights. (B) Numbers of mountains having dark slopes indicated in the scatterplot are shown on a similar horizontal scale.

3.3. Validation

In the absence of reliable (and co-located) measurements of elevation as "ground truth" it is difficult to prove that radarclinometry yields the correct results for mountain heights. One indirect confirmation comes from the study of channel systems. Radarclinometric estimates of the inward-facing slopes on the walls of channels in the 440 km crater Menrva (Kirk et al., 2005) were similar to the inward slopes of channels measured by stereoanalysis of Huygens DISR images (Tomasko et al., 2005). It should be noted, however, that the channels studied by the two techniques are distant from one another and differ by an order of magnitude in scale. Another check on the validity of heights from radarclinometry will come from radar stereo. As of this writing, the first radar stereopairs have been obtained (Elachi et al., 2006b) and the effort to measure topography is just beginning. Preliminary results suggest that mountains 500–1500 m high are present. Again, these estimates, which are subject to revision, are for areas far from the mountains described in the present paper. Nonetheless, the overlap in feature heights is encouraging. A final point concerning the absolute relief of mountains is that the greatest possible error, which would result if the mountains obeyed a steep backscatter law rather than a diffuse, cosine-like scattering law, has been shown to be about a factor of two. Given the strong evidence for very diffuse scattering in Xanadu and the similar brightness of mountains elsewhere, it is improbable that our chosen backscatter model is so far in error. Thus, our estimated mountain heights should be accurate to much better than a factor of two, perhaps to a few tens of percent.

A separate way to assess the reliability of our method addresses internal consistency and sensitivity to radar speckle noise, rather than absolute height accuracy, by plotting adjacent pixel traces on the same graph. Fig. 9 is a 3-D projection of

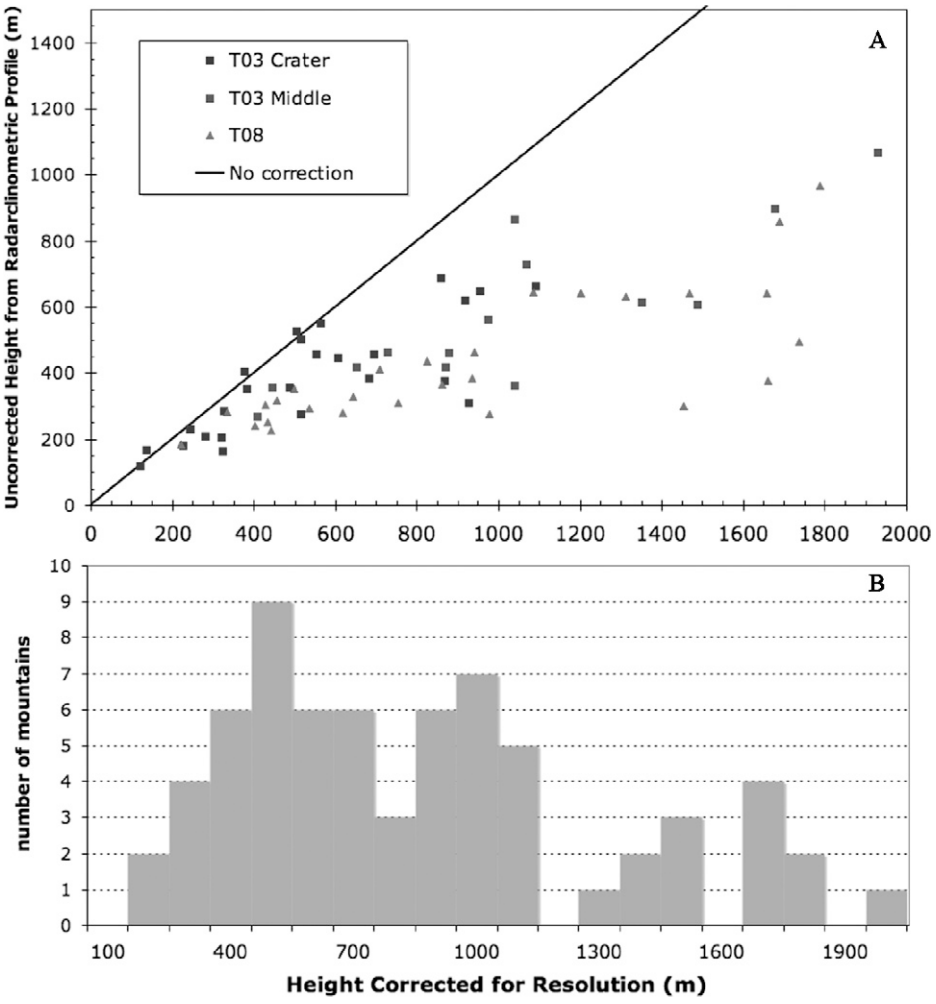

Fig. 8. (A) Maximum mountain uncorrected heights from radarclinometry (using a cosine backscatter law) on the vertical axis are plotted against maximum mountain heights corrected for resolution effects. Mountains in the T3 crater region are lower than those found in other regions, and due to having smaller slopes, also plot closer to the correlation line for the radarclinometry model and corrected heights. (B) Numbers of mountains found at those preferred, corrected heights are shown below on a similar horizontal scale.

seven adjacent pixel traces, each pixel spanning 175 m. It seems likely that the differences between adjacent profiles primarily reflect real topographic variations rather than being dominated by errors from noise in the image or other sources. As shown in Fig. 9, such inter-profile differences are slightly larger but generally comparable to pixel-to-pixel differences within the profiles. For example, the mean within-profile pixel-to-pixel difference is 16 m, while the mean across-profile difference is 60 m, although this is weighted by a few large difference values. Like the within-profile differences, cross-profile differences do exceed 100 m (corresponding to a 30° slope), but only rarely.

4. Mountain formation scenarios

The mountains on Titan are presumably made up of water ice, which is expected from cosmochemical abundance considerations and water's ubiquity in the Saturn system (Cruikshank et al., 2005). Titan's Voyager-measured density indicates that water ice makes up about 60% of Titan's mass (Sohl et al., 1995). This exists in a shell of water, with liquid overlain by a solid ice crust, that in turn overlies a silicate core (Lunine and Stevenson, 1987; Sohl et al., 1995). Groundbased spectroscopy (e.g., Griffith et al., 2003) appears to support the presence of water ice, although the analysis of data from the Cassini Visual and Infrared Mapping Spectrometer (VIMS; e.g., McCord et al., 2006) does not find a good match in water ice for the spectrum of Titan's bright surface features. At Titan's low surface temperature of 94 K ice behaves mechanically much as silicate rocks on Earth. It can support high topography features, especially on small horizontal distance scales. However, very high (>few km) topography on continent (>100 km) scales would lead to high lithostatic loads and elevated subsurface temperatures which would cause a structure to flow (Perron and de Pater, 2004) or, in an extreme case, may cause reorientation of the satellite along the Saturn gravity gradient (Smith et al., 1996). The mountains we observe, 10–20 km across and only a few hundred meters high, would not deform appreciably on geological timescales due to viscous flow at Titan's surface temperature. The geology discussed below assumes that the mountains are mainly composed of water ice.

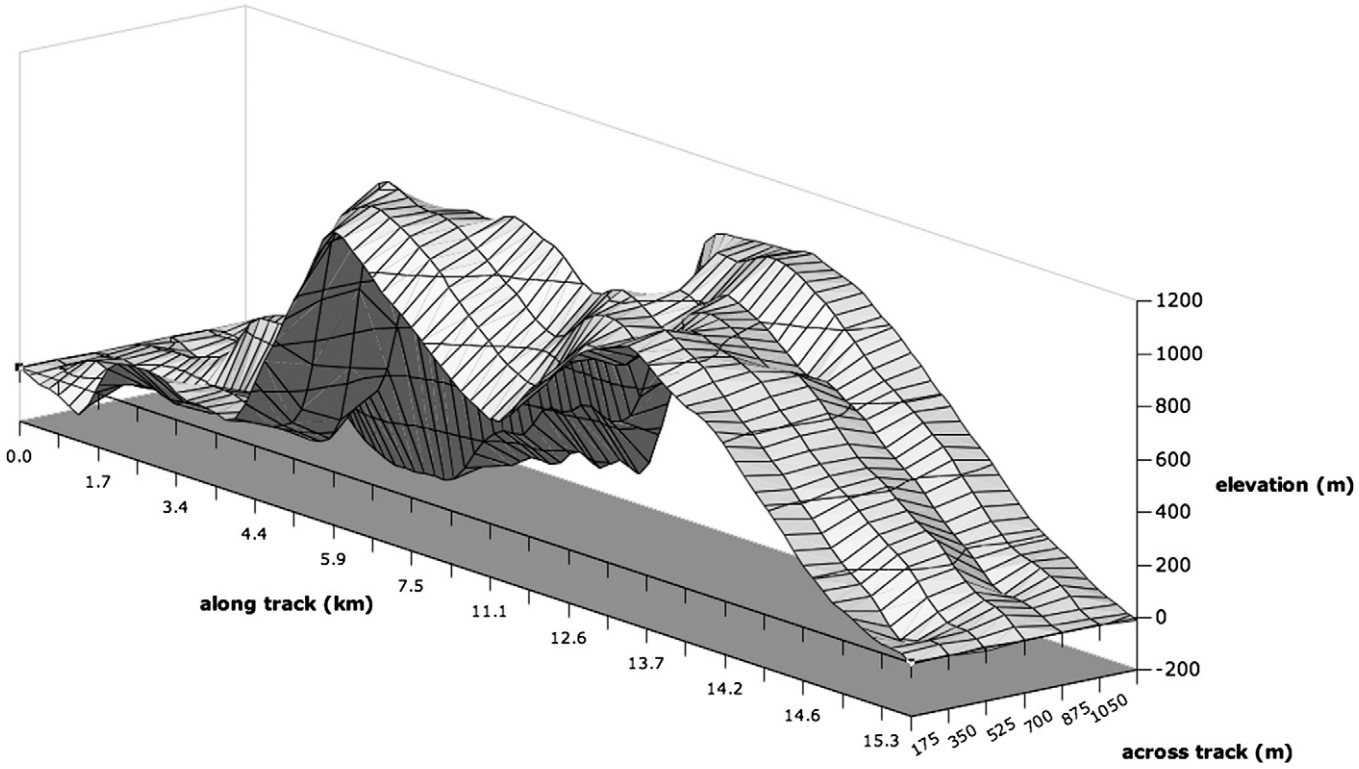

Fig. 9. Adjacent mountain traces merged to form a single 3-D range. This graph serves to illustrate the morphology of the mountain range. Maximum elevation is 1020 m, trace length is just over 15 km, and distance between adjacent pixels is 175 m. There is vertical and lateral exaggeration.

Four major scenarios for mountain formation are proposed here. 1—The blocks were thrust up from below due to crustal compression, 2—the crust has separated through extension, and has left high-standing blocks next to downdropped grabens, 3—blocks have been emplaced as secondary impact ejecta, and 4—a preexisting layer of material was stripped away to leave mesas and pinnacles. Mountains in all scenarios are then subject to erosion (likely dominated by hydrocarbon rainfall) and evolve to eroded peaks and surrounding blankets of material. Each scenario is considered below. We favor scenario 1 for the mountains in T8 and in T3 Area B (Figs. 4 and 5) because their linear-like traces are reminiscent of mountain chains across the solar system that have been created by compression. We briefly consider scenario 2, but do not find extensive evidence for it, we consider the possibility of scenario 3 for the mountains in T3 Area A (Figs. 4 and 5), and briefly discuss scenario 4 for some mountainous regions.

4.1. Mountain formation through compressional tectonism

The linear morphology of the mountain chains seen in the T8 study area and the middle of the T3 swath (Area B) is similar to that of mountain belts that are formed by lateral, compressional forces on the Earth and other planets (Figs. 3 and 5). Thus, we consider the possibility that compression has occurred in Titan's crust, leading to buckling and upthrusting of crustal blocks. This could be via either a complex fold-thrust or simple thrust-buckling mechanism. We note that the mountains on Titan are much larger than, and otherwise do not resemble, features found on other planets due to small-scale thrust faulting, such as sinuous wrinkle ridges. They also do not resemble ridge belts on Venus, which have simple bright/dark pair associations and have been interpreted to be folds (Solomon et al., 1992). In fact, we see no evidence of folds of any kind on Titan. Rather, the mountains resemble radar images of eroded mountains on Earth of various mechanisms of origin (see Fig. 3). Therefore, the key morphologic controller for mountains on Earth and perhaps Titan is erosion, which is discussed below.

Here we address the broader model of compression (either fold-thrust or simple thrust-buckling) for the formation of mountains on Titan. Although Titan has a much lower mass of rock than does the Earth, it is thought to have enough internal heat from radioactive decay and accretional energy, with a minor contribution (about 10%) of tidal heat from interaction with Saturn (Lorenz and Lunine, 2005), to enable at least solid state convection in its interior (Stevenson, 1992). Compression of the crust may be a result of global effects, such the progressive thickening of Titan's water ice crust associated with the cooling of the body, manifested as localized compression due to preexisting fault structures in the crust. Alternatively, if the crust has thickened relatively recently and begun to convect (Tobie et al., 2006), then diapirism could produce extension in some locations and compression in others. Additionally, as on Europa, tidal stresses within Titan may lead to surficial topographic features (Sohl et al., 1995). Many of Titan's mountain chains are 200–300 km long, which indicates that if lateral, compressive forces have built those mountains, they extended at least that far horizontally.

If portions of Titan's crust underwent compression leading to blocks of high-standing topography, these blocks would then

be subjected to the erosional processes occurring on Titan. Although the mechanical work that Titan's internal heat flow can perform is ∼100 times less in terms of watts per square meter than on Earth (Lorenz and Lunine, 2005), the corresponding erosive forces are ∼1000 times less (Lorenz and Lunine, 2005), and thus the construction of tectonic features may occur quickly enough to generate appreciable topography before erosion removes it. Also, possibly as much as 100–200 m worth of photochemical debris has rained out onto Titan's surface over the billion years that corresponds roughly to Titan's surface age (Lunine et al., 2005). Some fraction of this has covered portions of the younger mountain ranges. This makes it more difficult to unravel the history of the features, and we are left to estimate the amount of lateral crustal shortening, or strain. Some preliminary numbers are discussed in Section 5.

4.2. Mountain emplacement through extensional tectonism

A prominent geologic region in the US desert southwest, the Basin and Range Province, is formed by lateral crustal extension. This leaves high-standing mountain ranges or horsts, that have previously been compressed and folded, typically linear in planform perpendicular to the direction of extension. These are flanked by low-lying, linear graben. We consider this scenario for the mountains on Titan, since many of the mountain range tops have a linear trace. In addition, crustal extension typically occurs in the history of an icy Solar System body, as is evidenced by extensive fractures in most icy satellites. Recall from Section 4.1 that the Tobie et al. (2006) model predicts recent crustal thickening, which could result in extension in some locations. Although there are linear mountain ranges on Titan, there do not appear to be accompanying downdropped valleys, as are common on the Earth and Mars. In the T8 region, there are two weakly parallel ranges, an association seen strongly in the Basin and Range and in banded terrains on Ganymede and Europa, where extensional tectonics are likely responsible for the topography (Pappalardo et al., 1998). Linear, sub-parallel ranges and accompanying graben are not seen convincingly in the T3 or other mountain study regions thus far, so the scenario of crustal extension and associated formation of horsts and grabens may not be likely for these regions. However, the lack of evidence of graben might be a result of burial or modification, so we will continue to consider this model for the T8 region and other mountainous regions that will be discovered.

As an aside, although we do not propose an origin analogous to the Basin and Range for the features described in this paper, we may note that the length, width and height of the features, especially those in T8, are very comparable with some small mountain ranges in the southwest Basin and Range, such as the Harcuver Mountains (50 km long, ∼5 km wide and with highest peaks above the floor of about 700 m). The Gila Mountains and Maricopa Mountains are similar or slightly smaller.

4.3. Mountain emplacement as ejecta blocks

The association of the mountains with the 80 km crater Sinlap is striking, and although an origin as ejecta blocks may be surprising, consideration of the relevant ballistics establishes this as at least a possible origin. The mountains are at a range of around 200 km from the crater center: on a flat, airless Titan this would require a launch velocity of only about 500 m/s. For a typical mountain of ∼10 km across by 300 m high, the volume of material corresponds to a 2–3 km block, or slightly larger if the surrounding, erosional blanket is included (see Section 5). Inspection of secondary craters on the lunar surface (Vickery, 1986) shows that at least one block from the Copernicus crater was 2 km across and was launched at 500 m/s. 1000 m sized blocks of limestone are known around the 25 km Ries crater in Germany (Melosh, 1986). Even for high velocity impacts on present-day Titan, materials are rapidly decelerated by the atmosphere and deposited near the crater (Artemieva and Lunine, 2005). Mountains 3 and 4, 160–200 km away from Sinlap (Fig. 4A), are together oriented approximately radial to the crater, which supports the hypothesis that this is the source. It may be that in the low gravity and dense atmosphere of Titan, ejecta blocks are uniquely preserved, i.e., the block impact speeds are appreciably less than their launch speeds due to atmospheric drag. Blocks may be deposited, somewhat crushed on impact, but without enough energy to excavate a new secondary crater.

4.4. Mountain formation through layer removal

Processes on Mars and other bodies have acted to remove layers of material, exposing preexisting surfaces beneath them (e.g., Malin and Edgett, 2000; Head et al., 2003). Evidence for these processes includes incision and subsequent enlargement of drainage basins and dissection of easily eroded materials into patterned terrain. Likely compositions of these easily eroded materials on Mars and Earth are volcanic airfall deposits or fine, windblown materials. It is possible that these morphologies are seen in the bright, hilly terrain in the T7 swath in the deep southern hemisphere and the T13 swath that covers the leading-face bright region Xanadu. There are several dozen well-developed drainage networks in regions of T7 and T13, and many of those rivers meander through mountainous regions (Lunine et al., 2007). Some of the mountainous areas are rough and closely spaced, with many small peaks. These regions may be similar to areas in the Colorado Plateau, such as Bryce Canyon, wherein large, flat layers have been jointed and then eroded by water and sediment transport into drainages, knobs, and hoodoos (Lorenz and Lunine, 2005).

5. Volume considerations and erosion rates to obtain mountain ages

We can use simple volume considerations to estimate the total volume of a mountain block and from this obtain an approximate age of the feature. Mountains in our study areas are typically surrounded by radar-bright, diffuse blankets of material, often to several tens of kilometers from the mountain base. These are materials that have perhaps been eroded off the mountains and then deposited in a gently sloping mantle

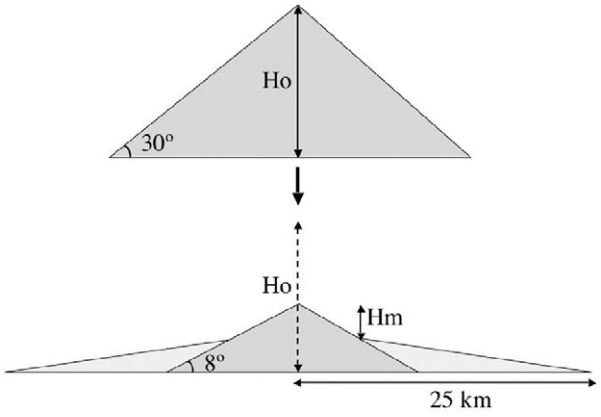

Fig. 10. Evolution of a mountain block into an eroded block with a surrounding blanket. Both the original block and final block with blanket have equivalent volumes that correspond to a cumulative upward displacement H_o. The measured mountain height H_m spans the summit and the contact of the mountain base with the erosional blanket.

that becomes thinner with greater radial distance. The blankets do not appear to have substantial topography or raised edges, so we consider the slopes of the blankets to be 2° or less.

We consider a mountain of a typical measured height (H_m) 300 m and slope 8° (Fig. 10). This mountain has a total horizontal extent of 10 km, and is surrounded by a blanket that extends 20 km from the mountain base in all directions and has a slope of 2°. The combined volumes of the mountain block and the blanket are equivalent to the total volume of the mountain block without erosion, assumed to be a conical block with slopes equal to the angle of repose, or 30°, thrust up via tectonism, of height H_o. (This assumes there has been no appreciable density change in the eroded material, and that material has not been carried far distant from the mountain location.) For the above values, the corresponding total volume is 570 km^3 and the cumulative upward displacement H_o is 5.7 km. This height corresponds very roughly to 1–2× this amount of lateral crustal shortening or horizontal strain, depending on the mode of upthrusting or buckling.

Mountain-building forces act to construct topography as erosional forces act to destroy it, resulting, as on Earth, in a landscape that is a dynamic equilibrium between these processes. When one or the other processes stops, the equilibrium is disrupted, as for example in the Appalachians on Earth, where erosion is currently dominating. Also on Titan, erosion seems to act fast enough (or mountain-building slow enough) to preclude the formation of abundant features taller than a few hundred meters. Indeed, the altimetric observations by the Cassini Radar (Elachi et al., 2005; Callahan et al., 2007) so far indicate a rather flat surface overall, despite the isolated structures discussed in this paper. Alternatively, the lack of extensive topographic features could be the result of a steep thermal gradient through most of Titan's history (Tobie et al., 2006), leading to topographic relaxation of features.

Terrestrial rainfall on a mountain top acts to produce a typical erosional rate of 0.5–1 mm yr^{-1} (Summerfield and Hulton, 1994). A study of channel erosion on Titan by Collins (2005) revealed that although materials are different (Titan's substrate is likely water ice and its liquids are methane or similar, while Earth's substrate is silicates and liquids are water), erosion rates on short timescales are similar on Earth and Titan (also Lorenz, 2000). Erosion rates over the long-term, however, depend most strongly on rates of precipitation. Since precipitation on Titan is likely more rare than on Earth (Lorenz and Lunine, 2005), we estimate a rate of erosion for our model mountain on Titan to be 10–25% the typical erosion rate on Earth mentioned above. We therefore estimate that it would take 20–100 million years to remove 5 km of topography and distribute it to the surrounding terrain, leaving the 2-km high mountain features observed. Thus, we speculate that this is a very approximate "age" of a typical mountain observed on Titan.

6. Distribution on Titan's surface and implications for global processes

Mountains of various morphologies and associations have been observed on the ∼15% of Titan's surface imaged so far at better than 1 km pixel^{-1} resolution. Regions containing mountains within the T3 and T8 swaths amount to about 0.5% of Titan's surface, and if we include the mountainous regions in swaths up to T20 (October 2006), mountains cover over 1% of Titan's surface (these numbers refer to regions delineated in Fig. 4, and thus include both mountains and flat plains between blocks and ranges, and other regions such as Xanadu not shown in figures). Measurements of 67 features in the T3 and T8 swaths have yielded heights from shape-from-shading up to 1930 m corrected for resolution effects, and a mean maximum slope of 37.2°. Mountains are found in such widely varying locations around Titan (latitudes 20° N, 0° N, 10° S, and 20° S, and longitudes 20° W, 40° W, 100° W, and 200° W) that it may be that the processes that form them are globally dispersive, although this possibility must be regarded as provisional, pending further radar imaging. Mountainous areas do not have broad, regional extents, but rather exist as isolated blocks or ranges within flat, low-lying plains (an exception to this may be the T13 Xanadu region, which will be explored in more detail in a future publication). If internal processes have occurred to raise these mountain blocks, the processes have been fairly localized. The worn appearance of the mountain peaks and the presence of surrounding blankets of materials indicate that erosion has been or currently is an active process on Titan. Volume considerations have enabled us to estimate an age of a typical mountain on Titan to be between 20 and 100 million years. This is short for planetary geological timescales, and further corroborates the conclusion from the dearth of impact craters (Elachi et al., 2005, 2006a; Wood et al., 2005; Lorenz et al., 2007b) that the surface overall is less than a billion years old.

Acknowledgments

We thank Richard Ghail and an anonymous reviewer for their careful reading of and useful commenting on the manuscript. The authors are supported at least in part by the Cassini

mission. We gratefully acknowledge those who designed, developed and operate the Cassini mission, which is a joint endeavor of the National Aeronautics and Space Administration (NASA), the European Space Agency (ESA), and the Italian Space Agency (ASI) and is managed by JPL/Caltech under a contract with NASA.

References

Artemieva, N., Lunine, J., 2005. Impact cratering on Titan. II. Global melt, escaping ejecta, and aqueous alteration of surface organics. Icarus 175, 522–533.

Boubin, G.M., Reffet, E.G., Lunine, J.I., Radebaugh, J., Lopes, R.M., and the Cassini Radar Team, 2005. Mapping and characterization of "cat scratches" on Titan. Bull. Am. Astron. Soc. 37. Abstract 46.04.

Callahan, P.S., Hensley, S., Gim, Y., Johnson, W.T., Lorenz, R.D., Alberti, G., Orosei, R., Seu, R., Franceschetti, G., Paillou, P., Paganelli, F., Wall, S., West, R.D., 2006. Information on Titan's surface from Cassini Radar Altimeter waveforms. Eos Trans. AGU (Fall Suppl.) 87 (52). P13A-0165.

Callahan, P.S., Lorenz, R., Gim, Y., Alberti, G., Flamini, E., Seu, R., Picardi, G., Orosei, R., Zebker, H., Lunine, J., Hamilton, G., Hensley, S., Johnson, W.T.K., Shaffer, S., Wall, S., West, R., Francescetti, G., 2007. Titan's topography: Initial results from the Cassini RADAR Altimeter. J. Geophys. Res. Planets, submitted for publication.

Collins, G.C., 2005. Relative rates of fluvial bedrock incision on Titan and Earth. Geophys. Res. Lett. 32, doi:10.1029/2005GL024551. L22202.

Cruikshank, D.P., Owen, T.C., Dalle Ore, C., Geballe, T.R., Roush, T.L., De Bergh, C., Sandford, S.A., Poulet, F., Benedix, G.K., Emery, J.P., 2005. A spectroscopic study of the surfaces of Saturn's large satellites: H_2O ice, tholins and minor constituents. Icarus 175, 268–283.

Elachi, C., Wall, S., Allison, M., Anderson, Y., Boehmer, R., Callahan, P., Encrenaz, P., Flameni, E., Francescetti, G., Gim, Y., Hamilton, G., Hensley, S., Janssen, M., Johnson, W., Kelleher, K., Kirk, R., Lopes, R., Lorenz, R., Lunine, J., Muhleman, D., Ostro, S., Paganelli, F., Picardi, G., Posa, F., Roth, L., Seu, R., Shaffer, S., Soderblom, L., Stiles, B., Stofan, E., Vetrella, S., West, R., Wood, C., Wye, L., Zebker, H., 2005. Cassini Radar views the surface of Titan. Science 308, 970–974.

Elachi, C., Wall, S., Janssen, M., Stofan, E., Lopes, R., Kirk, R., Lorenz, R., Lunine, J., Paganelli, F., Soderblom, L., Wood, C., Wye, L., Zebker, H., Anderson, Y., Ostro, S., Allison, M., Boehmer, R., Callahan, P., Encrenaz, P., Flameni, E., Francescetti, G., Gim, Y., Hamilton, G., Hensley, S., Johnson, W., Kelleher, K., Muhleman, D., Picardi, G., Posa, F., Roth, L., Seu, R., Shaffer, S., Stiles, B., Vetrella, S., West, R., 2006a. Titan Radar Mapper observations from Cassini's T3 fly-by. Nature 441, 709–713.

Elachi, C., Wall, S., Lopes, R., Soderblom, L., Lunine, J., Lorenz, R., Janssen, M., Kirk, R., and the Cassini Radar Team, 2006b. Titan's surface by Radarlight. Bull. Am. Astron. Soc. 38. Abstract 48.01.

Friedson, A.J., 1994. Gravity waves in Titan's atmosphere. Icarus 190, 40–57.

Griffith, C.A., Owen, T., Geballe, T.R., Rayner, J., Rannou, P., 2003. Evidence for the exposure of water ice on Titan's surface. Science 300, 628–630.

Gupta, R.P., Fritz, H., Bojar, A.-V., 2006. Cover: On the nature of the South Tibetan Detachment Zone (STDZ), Kumaun Himalayas. Int. J. Rem. Sens. 27, 455–458.

Head, J.W., Mustard, J.F., Kreslavsky, M.A., Milliken, R.E., Marchant, D.R., 2003. Recent ice ages on Mars. Nature 426, 797–802.

Kirk, R.L., 1987. A fast finite-element algorithm for two-dimensional photoclinometry. Thesis, California Institute of Technology, Pasadena, CA. Part III, pp. 165–258.

Kirk, R.L., Radebaugh, J., 2007. Resolution effects in radarclinometry. In: ISPRS WG IV/7: Extraterrestrial Mapping Workshop, Abstracts.

Kirk, R.L., Callahan, P., Seu, R., Lorenz, R.D., Paganelli, F., Lopes, R.M., Elachi, C., and the Cassini Radar Team, 2005. Radar reveals Titan topography. Lunar Planet. Sci. XXXVI, 2227. Abstract.

Kirk, R.L., Wall, S.D., Lorenz, R.D., Lunine, J.I., Radebaugh, J., Soderblom, L.A., Stiles, B.W., Janssen, M.A., Paganelli, F., Lopes, R., and the Cassini Radar Team, 2006. A high resolution view of the Xanadu region of Titan from the Cassini Radar. Bull. Am. Astron. Soc. 38. Abstract 52.03.

Lopes, R., Mitchell, K.L., Stofan, E.R., Lunine, J.I., Lorenz, R., Paganelli, F., Kirk, R.L., Wood, C.A., Wall, S.D., Robshaw, L.E., Fortes, A.D., Neish, C.D., Radebaugh, J., Reffet, E., Ostro, S.J., Elachi, C.D., Allison, M., Anderson, Y., Boehmer, R., Boubin, G., Callahan, P., Encrenaz, P., Flamini, E., Francescetti, G., Gim, Y., Hamilton, G., Hensley, S., Janssen, M.A., Johnson, W.T., Kelleher, K., Muhleman, D.O., Ori, G., Orosei, R., Picardi, G., Posa, F., Roth, L.E., Seu, R., Shaffer, S., Soderblom, L.A., Stiles, B., Vetrella, S., West, R.D., Wye, L., Zebker, H.A., 2007. Cryovolcanic features on Titan's surface as revealed by the Cassini Titan Radar Mapper. Icarus 186, 395–412.

Lorenz, R.D., 2000. The weather on Titan. Science 290, 467–468.

Lorenz, R.D., Lunine, J.I., 2005. Titan's surface before Cassini. Planet. Space Sci. 53, 557–576.

Lorenz, R., Mitton, J., 2002. Lifting Titan's Veil. Cambridge Univ. Press, Cambridge.

Lorenz, R.D., Wall, S.D., Reffet, E., Boubin, G., Radebaugh, J., Elachi, C., Allison, M.D., Anderson, Y., Boehmer, R., Callahan, P., Encrenaz, P., Flamini, E., Francescetti, G., Gim, Y., Hamilton, G., Hensley, S., Janssen, M.A., Johnson, W.T., Kelleher, K., Kirk, R.L., Lopes, R.M., Lunine, I.J., Mitchell, K., Muhleman, D.O., Ori, G., Orosei, R., Ostro, S.J., Paganelli, F., Picardi, G., Posa, F., Roth, L.E., Seu, R., Shaffer, S., Soderblom, L.A., Stiles, B., Stofan, E.R., Vetrella, S., West, R.D., Wye, L., Zebker, H.A., 2006a. Radar Imaging of giant longitudinal dunes: Namib Desert (Earth) and the Belet Sand Sea (Titan). Lunar Planet. Sci. XXXVII, 1249. Abstract.

Lorenz, R.D., Wall, S., Radebaugh, J., Boubin, G., Reffet, E., Janssen, M., Stofan, E., Lopes, R., Kirk, R., Elachi, C., Lunine, J., Paganelli, F., Soderblom, L., Wood, C., Wye, L., Zebker, H., Anderson, Y., Ostro, S., Allison, M., Boehmer, R., Callahan, P., Encrenaz, P., Ori, G.G., Francescetti, G., Gim, Y., Hamilton, G., Hensley, S., Johnson, W., Kelleher, K., Mitchell, K., Muhleman, D., Picardi, G., Posa, F., Roth, L., Seu, R., Shaffer, S., Stiles, B., Vetrella, S., Flamini, E., West, R., 2006b. The sand seas of Titan: Cassini Radar observations of longitudinal dunes. Science 312, 724–727.

Lorenz, R.D., Lopes, R.M., Paganelli, F., Lunine, J.I., Kirk, R.L., Soderblom, L.A., Stofan, E., Ori, G., Myers, M., Miyamoto, H., Stiles, B., Wall, S.D., Wood, C.A., and the Cassini Radar Team, 2007a. Fluvial channels on Titan: Meteorological paradigm and Cassini Radar observations. Planet. Space Sci., in press.

Lorenz, R.D., Wood, C.A., Lunine, J.I., Wall, S.D., Lopes, R.M., Mitchell, K.L., Paganelli, F., Anderson, Y.Z., Wye, L., Tsai, C., Zebker, H.R., Stofan, E., and the Cassini Radar Team, 2007b. Titan's young surface: Initial impact crater survey by Cassini Radar and model comparison. Geophys. Res. Lett. 34, doi:10.1029/2006GL028971. L07204.

Lunine, J.I., Stevenson, D.J., 1987. Clathrate and ammonia hydrates at high pressure—Application to the origin of methane on Titan. Icarus 70, 61–77.

Lunine, J.I., Artemieva, N., Lorenz, R., Flamini, E., 2005. Numerical modeling of impact cratering on Titan with implications for the age of Titan's surface. Lunar Planet. Sci. XXXVI, 1504. Abstract.

Lunine, J.I., Elachi, C., Wall, S.D., Allison, M.D., Anderson, Y., Boehmer, R., Callahan, P., Encrenaz, P., Flamini, E., Franceschetti, G., Gim, Y., Hamilton, G., Hensley, S., Janssen, M.A., Johnson, W.T.K., Kelleher, K., Kirk, R.L., Lopes, R.M., Lorenz, R., Muhleman, D.O., Orosei, R., Ostro, S.J., Paganelli, F., Paillou, P., Picardi, G., Posa, F., Radebaugh, J., Roth, L.E., Seu, R., Shaffer, S., Soderblom, L.A., Stiles, B., Stofan, E.R., Vetrella, S., West, R., Wood, C.A., Wye, L., Zebker, H., Alberti, E., Karkoschka, B., Rizk, G., McFarlane, E., Kazeminejad, B., 2007. Titan's diverse landscapes as evidenced by Cassini RADAR third and fourth looks at Titan. Icarus, submitted for publication.

Malin, M.C., Edgett, K.S., 2000. Sedimentary rocks of early Mars. Science 290, 1927–1937.

McCord, T.B., Hansen, G.B., Buratti, B.J., Clark, R.N., Cruikshank, D.P., D'Aversa, E., Griffith, C.A., Baines, K.H., Brown, R.H., Dalle Ore, C.M., Filacchione, G., Formisano, V., Hibbitts, C.A., Jaumann, R., Lunine, J.I., Nelson, R.M., Sotin, C., and the Cassini Vims Team, 2006. Titan: Surface composition from Cassini VIMS. Lunar Planet. Sci. XXXVII, 1398. Abstract.

Melosh, H.J., 1986. Impact Cratering. Oxford Univ. Press, Oxford.

Paganelli, F., Janssen, M.A., Stiles, B., West, R., Lorenz, R.D., Lunine, J.I., Lopes, R.M., Stofan, E., Kirk, R.L., Roth, L., Wall, S.D., Elachi, C., and

the Cassini Radar Team, 2007a. Titan's surface from the Cassini Radar SAR and high resolution radiometry data of the first five flybys. Icarus, doi:10.1016/j.icarus.2007.04.032, in press.

Paganelli, F., Janssen, M.A., Lopes, R.M., Stofan, E., Wall, S.D., Lorenz, R.D., Lunine, J.I., Kirk, R.L., Roth, L., Elachi, C., and the Cassini Radar Team, 2007b. Titan's surface from the Cassini Radar radiometry data during SAR mode. Planet. Space Sci. Special Issue EGU 2006, in press.

Pappalardo, R.T., Head, J.W., Collins, G.C., Kirk, R.T., Neukum, G., Oberst, J., Geist, B., Greeley, R., Chapman, C.R., Helfenstein, P., Moore, J.M., McEwen, A.S., Tufts, B.R., Senske, D.A., Breneman, H.H., Klaasen, K., 1998. Grooved terrain on Ganymede: First results from Galileo high-resolution imaging. Icarus 135, 276–302.

Perron, J.T., de Pater, I., 2004. Dynamics of an ice continent on Titan. Geophys. Res. Lett. 31, doi:10.1029/2004GL019802. L17S04.

Porco, C.C., Baker, E., Barbara, J., Beurle, K., Brahic, A., Burns, J.A., Charnoz, S., Cooper, N., Dawson, D.D., Del Genio, A.D., Denk, T., Dones, L., Dyudina, U., Evans, M.W., Fussner, S., Giese, B., Grazier, K., Helfenstein, P., Ingersoll, A.P., Jacobson, R.A., Johnson, T.V., McEwen, A., Murray, C.D., Neukum, G., Owen, W.M., Perry, J., Roatsch, T., Spitale, J., Squyres, S., Thomas, P., Tiscareno, M., Turtle, E.P., Vasavada, A.R., Veverka, J., Wagner, R., West, R., 2005. Imaging of Titan from the Cassini spacecraft. Nature 434, 159–168.

Radebaugh, J., Lorenz, R., Kirk, R., Lunine, J., and the Cassini Radar Team, 2006. Mountains on Titan observed by Cassini Radar. Lunar Planet. Sci. XXXVII, 1007. Abstract.

Radebaugh, J., Lorenz, R., Lunine, J., Wall, S., Boubin, G., Reffet, E., Kirk, R., Lopes, R., Stofan, E., Soderblom, L., Allison, M., Janssen, M., Paillou, P., Callahan, P., and the Cassini Radar Team, 2007. Dunes on Titan observed by Cassini Radar. Icarus, in press.

Smith, P.H., Lemmon, M.T., Lorenz, R.D., Sromovsky, L.A., Caldwell, J.J., Allison, M.D., 1996. Titan's surface, revealed by HST imaging. Icarus 119, 336–349.

Sohl, F., Sears, W.D., Lorenz, R.D., 1995. Tidal dissipation on Titan. Icarus 115, 278–294.

Solomon, S.C., Smrekar, S.E., Bindschadler, D.L., Grimm, R.E., Kaula, W.M., McGill, G.E., Phillips, R.J., Saunders, R.S., Schubert, G., Squyres, S.W., Stofan, E.R., 1992. Venus tectonics: An overview of Magellan observations. J. Geophys. Res. 97, 13199–13256.

Stevenson, D.J., 1992. Interior of Titan. In: Proceedings Symposium of Titan, ESA SP-338. European Space Agency, Noordwijk, pp. 29–33.

Stofan, E.R., Senske, D.A., Michaels, G., 1993. Tectonic features in Magellan data. In: Ford, J. (Ed.), Guide to Magellan Image Interpretation. JPL Publication 93-24, Pasadena, CA.

Stofan, E.R., Lunine, J.I., Lopes, R., Paganelli, F., Lorenz, R.D., Wood, C.A., Kirk, R., Wall, S., Elachi, C., Soderblom, L.A., Ostro, S., Janssen, M., Radebaugh, J., Wye, L., Zebker, H., Anderson, Y., Allison, M., Boehmer, R., Callahan, P., Encrenaz, P., Flamini, E., Francescetti, G., Gim, Y., Hamilton, G., Hensley, S., Johnson, W.T.K., Kelleher, K., Muhleman, D., Picardi, G., Posa, F., Roth, L., Seu, R., Shaffer, S., Stiles, B., Vetrella, S., West, R., 2006. Mapping of Titan: Results from the first two Titan Radar passes. Icarus 185, 443–456.

Stofan, E.R., Elachi, C., Lunine, J.I., Lorenz, R.D., Stiles, B., Mitchell, K.L., Ostro, S., Soderblom, L., Wood, C., Zebker, H., Wall, S., Janssen, M., Kirk, R., Lopes, R., Paganelli, F., Radebaugh, J., Wye, L., Anderson, Y., Allison, M., Boehmer, R., Callahan, P., Encrenaz, P., Flamini, E., Francescetti, G., Gim, Y., Hamilton, G., Hensley, S., Johnson, W.T.K., Kelleher, K., Muhleman, D., Paillou, P., Picardi, G., Posa, F., Roth, L., Seu, R., Shaffer, S., Vetrella, S., West, R., 2007. The lakes of Titan. Nature 445, 61–64.

Summerfield, M.A., Hulton, N.J., 1994. Natural controls of fluvial denudation rates in major world drainage basins. J. Geophys. Res. 99, 13871–13883.

Tobie, G., Lunine, J.I., Sotin, C., 2006. Episodic outgassing as the origin of atmospheric methane on Saturn's moon Titan. Nature 440, 61–64.

Tokano, T., Lorenz, R.D., 2006. GCM simulation of balloon trajectories on Titan. Planet. Space Sci. 54, 685–694.

Tomasko, M.G., Archinal, B., Becker, T., Bézard, B., Bushroe, M., Combes, M., Cook, D., Coustenis, A., de Bergh, C., Dafoe, L.E., Doose, L., Douté, S., Eibl, A., Engel, S., Gliem, F., Grieger, B., Holso, K., Howington-Kraus, E., Karkoschka, E., Keller, H.U., Kirk, R., Kramm, R., Küppers, M., Lanagan, P., Lellouch, E., Lemmon, M., Lunine, J., McFarlane, E., Moores, J., Prout, G.M., Rizk, B., Rosiek, M., Rueffer, P., Schröder, S.E., Schmitt, B., See, C., Smith, P., Soderblom, L., Thomas, N., West, R., 2005. Rain, winds and haze during the Huygens probe's descent to Titan's surface. Nature 438, 765–778.

Vickery, A.M., 1986. Size–velocity distribution of large ejecta fragments. Icarus 67, 224–236.

Wood, C.A., Lopes, R.M., Stofan, E.R., Paganelli, F., Elachi, C., 2005. Impact Craters on Titan? Cassini Radar View. Lunar Planet. Sci. XXXVI, 1117. Abstract.

Wye, L.C., Zebker, H.A., Ostro, S.J., West, R.D., Gim, Y., Lorenz, R.D., and the Cassini Radar Team, 2007. Electrical properties of Titan's surface from Cassini Radar scatterometer measurements. Icarus 188, 367–385.